Akerman, S., Fisher, M., Daniel, R. A., Lefley, D. V., Reyes-Aldasoro, C. C., Lunt, S. J., Harris, S., Björndahl, M. A., Williams, L. J., Evans, H., Barber, P. R., Prise, V. E., Vojnovic, B., Kanthou, C. & Tozer, G. M. (2013). Influence of soluble or matrix-bound isoforms of vascular endothelial growth factor-A on tumor response to vascular-targeted strategies. International Journal of Cancer, 133(11), pp. 2563-2576. doi: 10.1002/ijc.28281

Influence of soluble or matrix-bound isoforms of vascular endothelial growth factor-A on tumor response to vascular-targeted strategies

[1,2,8]Simon Akerman, [1,8]Matthew Fisher, [1,8]Rachel A. Daniel, [1]Diane Lefley, [1,3]Constantino C. Reyes-Aldasoro, [1]Sarah Jane Lunt, [1]Sheila Harris, [1,4]Meit Bjorndahl, [1,5]Leigh J. Williams, [1]Helen Evans, [6]Paul R. Barber, [7]Vivien E. Prise, [6]Borivoj Vojnovic, [1]Chryso Kanthou and *[1]Gillian M. Tozer

[1]Tumor Microcirculation Group, CR-UK/YCR Sheffield Cancer Research Centre, University of Sheffield, F Floor, School of Medicine, Beech Hill Road, Sheffield, S10 2RX, UK

[2]Current address: Headache Group, Department of Neurology, University of California, San Francisco, Department of Neurology, 513 Parnassus Avenue, San Francisco, CA 94143-0114

[3]Current address: University of Sussex, Department of Engineering and Design, Biomedical Engineering Research Group, 2B10 Shawcross Building, BN1 9QT, Brighton, UK

[4]Current address: SentoClone International AB, Stockholm, Sweden

[6]Gray Institute for Radiation Oncology & Biology, University of Oxford, Old Road Campus Research Building, Off Roosevelt Drive, Churchill Hospital, Oxford, OX3 7DQ

[7]Centre for Vision & Vascular Science, Queen's University Belfast, Royal Victoria Hospital, Belfast, BT12 6BA, UK

[8] These authors contributed equally to the study

*Correspondence address:
Professor G. Tozer
Tumor Microcirculation Group
Department of Oncology
University of Sheffield
F Floor, School of Medicine
Beech Hill Road
Sheffield
S10 2RX
Email: g.tozer@sheffield.ac.uk
Tel: +44 114 2712834
Fax: +44 114 2713314

KEY WORDS: VEGF isoforms, vascular normalization, red cell velocity, receptor tyrosine kinase inhibitors, vascular disrupting agents

ARTICLE CATEGORY: Cancer Cell Biology

NOVELTY & IMPACT: Treatment-induced tumor vascular normalization is a common phenomenon but poorly understood. Differential VEGF isoform expression strongly influences vascular morphology and function. Using intravital microscopy, we found that the soluble 120 isoform of VEGF is associated with tumor susceptibility to vascular normalization induced by VEGFR-2-targeted treatment. Furthermore, normalization rendered tumor blood vessels resistant to subsequent treatment with the archetypal vascular disrupting agent, CA4P. Results suggest VEGF isoform expression can predict for tumor response to vascular-targeted therapy.

ABBREVIATIONS USED: ANOVA (analysis of variance); α-SMA (alpha smooth muscle actin); CA4P (combretastatin A4 3-*O*-phosphate); CD31 (cluster differentiation 31 / platelet endothelial cell adhesion molecule); c-RET (intrinsic re-arranged-during-transfection protein); DAB (3,3'-diaminobenzidine; DMEM (Dulbecco's minimal essential medium); DMSO (dimethyl sulfoxide); Flk1 (fetal liver kinase 1); Flt1 (Fms-like tyrosine kinase 1); Flt3 (Fms-like tyrosine kinase 3); GIST (gastro-intestinal stromal tumors); HRP (horseradish peroxidase); IFP (interstitial fluid pressure); KDR (kinase insert domain receptor) NSCLC (non-small cell lung cancer); PDGFR-β (platelet derived growth factor receptor beta); pERK (phosphorylated extra-cellular signal-regulated kinases); RCC (renal cell carcinoma); RCV (red cell velocity); RTK (receptor tyrosine kinase); SCID (severe combined immune deficient); stem cell growth factor receptor/c-Kit (SCF R), VDA (vascular disrupting agent); VEGF (vascular endothelial growth factor A); VEGFR-2 (VEGF receptor 2).

Abstract

Anti-angiogenic therapy based on blocking the actions of vascular endothelial growth factor-A (VEGF) can lead to 'normalization' of blood vessels in both animal and human tumors. Differential expression of VEGF isoforms affects tumor vascular maturity, which could influence the normalization process and response to subsequent treatment. Fibrosarcoma cells expressing only VEGF120 or VEGF188 isoforms were implanted either subcutaneously (s.c.) or in dorsal skin-fold 'window' chambers in SCID mice. VEGF120 was associated with vascular fragility and hemorrhage. Tumor-bearing mice were treated with repeat doses of SU5416, an indolinone receptor tyrosine kinase (RTK) inhibitor with activity against VEGFR-2 and proven pre-clinical ability to induce tumor vascular normalization. SU5416 reduced vascularization in s.c. implants of both VEGF120 and VEGF188 tumors. However, in the window chamber, SU5416 treatment increased red cell velocity in VEGF120 (representing vascular normalization) but not VEGF188 tumors. SU5416 treatment had no effect on growth or necrosis levels in either tumor type but tended to counteract the increase in interstitial fluid pressure (IFP) seen with growth of VEGF120 tumors. SU5416 pre-treatment resulted in the normally fragile blood vessels in VEGF120-expressing tumors becoming resistant to the vascular damaging effects of the tubulin-binding vascular disrupting agent (VDA), combretastatin A4 3-*O*-phosphate (CA4P). Thus, vascular normalization induced by anti-angiogenic treatment can reduce the efficacy of subsequent VDA treatment. Expression of VEGF120 made tumors particularly susceptible to vascular normalization by SU5416, which in turn made them resistant to CA4P. Therefore VEGF isoform expression may be useful for predicting response to both anti-angiogenic and vascular-disrupting therapy.

Supported by Cancer Research UK Programme Grant C1276/A9993

Introduction

Vascular endothelial growth factor-A (VEGF) is a key stimulator of tumor angiogenesis and the most well-studied target for anti-angiogenic therapy [1, 2]. Anti-VEGF monotherapy has been approved in a limited number of clinical settings, notably in advanced renal cell carcinoma. However, most success has been achieved by combining VEGF-targeted treatments with chemotherapeutic drugs [2]. VEGF inhibition can effectively block tumor angiogenesis and slow tumor growth in mouse models of cancer [3]. However, in animal models it has been shown also that there is a dose and time window at which vascular 'normalization' occurs following anti-angiogenic therapy, involving re-modelling of the vasculature resulting in improved delivery of oxygen and therapeutic drugs to tumor tissue [4, 5]. Detecting tumor vascular normalization in the clinic is challenging, requiring sophisticated imaging technology to monitor vascular morphology and function. Nevertheless, this phenomenon has been reported clinically with both the monoclonal antibody to VEGF, bevacizumab (Avastin; Genentech) [6], and the VEGF receptor tyrosine kinase (RTK) inhibitor, cediranib (Recentin; AstraZeneca) [7]. If vascular normalization proves to be a common phenomenon in human tumors during/following anti-angiogenic therapy, it could potentially explain the beneficial combination of anti-angiogenic treatment with chemotherapy and provide further possibilities for therapeutic exploitation. In order for rational therapeutic exploitation to occur, further information is required regarding the nature of this phenomenon and its influence on subsequent therapy.

RTK inhibitors form a large group of anti-cancer agents, many of them developed as anti-angiogenic agents targeted against VEGFR-2 (flk-1/KDR) but with a range of target specificities. SU5416 (semaxinib) is an indolinone, developed by Sugen as a

VEGFR-2 inhibitor, which binds to the tyrosine kinase domain of the receptor [8]. It acts as an ATP-mimetic and is the predecessor of SU11248 (sunitinib or Sutent), which is approved for treatment of renal cell carcinoma and imatinib-resistant gastrointestinal stromal tumors (GIST) as monotherapy. Experiments using both cell-free and cellular systems have shown that SU5416 inhibits other receptor tyrosine kinases, in addition to VEGFR-2, such as c-Kit, Flt3, c-MET and PDGFR, with variable potencies [8-11] although the complete specificity profile of SU5416, as for its related compounds, is unknown [12]. SU5416 has been withdrawn from clinical testing but is a useful exemplar of a class of RTK inhibitors with activity against VEGFR-2 and ability to induce tumor vascular normalization [13, 14].

It is increasingly recognised that differential gene-splicing of VEGF gives rise to variations in vascular patterning in both normal embryology [15] and tumor angiogenesis [16, 17]. The most prevalent VEGF protein isoforms consist of 121, 165 and 189 amino acids in the human and 120, 164 and 188 in the mouse [18]. These isoforms differ in molecular mass, solubility and heparin-binding affinity but all interact with the VEGF receptors, Flt1 (VEGFR-1) and Flk1/KDR (VEGFR-2) [19]. All three isoforms can be found in human tumor tissue, with VEGF121 (soluble isoform) and 165 commonly the most prevalent [20, 21]. Despite this prevalence, clinical studies suggest that the balance between all three isoforms is important for driving tumor angiogenesis and progression. For instance, matrix-bound VEGF189 expression has been reported to associate with increased vascularity, progression and prognosis in non-small-cell lung cancer (NSCLC), renal cell carcinoma (RCC) and colorectal carcinomas [22-24], whereas the soluble isoforms were reported to be associated with metastasis in melanoma and squamous cell carcinoma of the head and neck [25, 26]. There is mounting evidence that the different VEGF isoforms can differentially

signal, perhaps due to their diverse abilities to bind co-receptors of VEGFR-2 such as the neuropilins, integrins and heparan sulphate proteoglycans [27]. This implies that VEGF isoform expression could also influence response to specific treatments. However, little is known about this aspect of VEGF tumor biology and, in particular, nothing is known about how vascular patterning and function determines susceptibility to vascular normalization. Using mouse fibrosarcoma cell lines developed to express only single isoforms of VEGF under endogenous promoter control, we found that the corresponding solid tumors expressed the relevant isoforms and had disparate vascular characteristics, making them useful models for investigating factors associated with the process of vascular normalization induced by anti-angiogenic treatment[17].

The aims of the current study were i) to determine whether differential expression of individual VEGF isoforms (VEGF120 and VEGF188) which predicate for diverse tumor vascular morphology and function, is associated with differential susceptibility to normalization (morphological and functional end-points) following treatment with an archetypal receptor tyrosine kinase inhibitor (SU5416) and, if normalization occurs, ii) to determine how this process affects subsequent vascular susceptibility to disruption by a typical tubulin-binding VDA (CA4P). We reasoned that VEGF120-expressing tumors would be particularly susceptible to vascular normalization and that this would alter their response to CA4P.

Methods

All experiments were conducted in accordance with the United Kingdom Home Office Animals (Scientific Procedures) Act 1986, with local ethical approval and in

line with recently published guidelines [28]. CA4P was kindly provided by Professor GR Pettit, Arizona State University.

VEGF isoform-specific tumor cell lines

In-house-developed mouse fibrosarcoma cell lines, which produce only single isoforms of VEGF (120 and 188), under endogenous promoter control, were used in this study [17]. Cells were maintained in high glucose DMEM (Invitrogen, Paisley, UK) media containing L-glutamine, fetal calf serum, and the antibiotics G-418 and puromycin. Previous investigations showed that only the relevant VEGF isoforms were produced from each isoform-specific cell line [17].

Subcutaneous tumor transplantation and tumor growth

1 x 10^6 tumor cells in 0.05 ml were injected subcutaneously on the rear dorsum of severe combined immunodeficient (SCID) mice (8-12 week-old, 20-25g). Animals were grouped and treated with either a tyrosine kinase receptor inhibitor, SU5416 (50 mg/kg, i.p), or drug vehicle (DMSO, 0.05 ml, i.p) every 3rd to 4th day (twice per week), starting on day 4 after tumor implantation). Caliper measurements were made to calculate tumor volume, V, where V = 0.52 x d1 x d2 x d3 and d1, d2 and d3 are the three orthogonal tumor diameters. Animals were sacrificed when the largest tumor diameter reached ~12 mm.

Immunohistochemistry and histology

Tumor-bearing mice were treated with SU5416 or vehicle, as described above, when tumors reached 6-7 mm in diameter. Some mice also received CA4P (100 mg/kg at 10 ml/kg i.p.) or saline vehicle, 21 h after the second dose of SU5416.

Tumors were excised 6, 24 or 48 h after the second dose of SU5416/vehicle and halved for zinc or formalin fixation or frozen in isopentane on dry ice. 2.5 hours prior to tumor excision in the 24 h group, mice received 60 mg/kg pimonidazole HCl (HypoxyProbe Kit, HPI Inc, Burlington, MA, USA) at 10 ml/kg i.p. for analysis of tumor hypoxia [29].

5 μm thick sections from the centre of fixed paraffin-embedded tumor samples were stained for endothelial cells using rat anti-mouse CD31 monoclonal antibodies (Cat no. 557355, BD Pharmingen Intl, Oxford, UK for zinc-fixed or Cat No. DIA-310, Dianova GmbH, Hamburg, Germany for formalin-fixed tissue). The HydroxyProbe kit was used to identify pimonidazole-protein adducts formed under severe hypoxia. Heat/pressure and microwave antigen retrieval were used for CD31 and pimonidazole staining respectively. Sections were exposed to the primary antibody overnight at 4°C and standard signal amplification was achieved using an avidin-biotin complex (ABC)/horseradish peroxidase system (Vectastain, Vector Laboratories, Burlingame, CA, USA). The signal was visualized with DAB (Dako, Ely, UK) and sections were counterstained with haematoxylin.

CD31 staining in viable tumor regions was quantitatively analysed using an in-house-developed segmentation algorithm to determine morphological characteristics of tumor vasculature [30]. Additional formalin-fixed sections were stained with haematoxyin and eosin for necrosis scoring, whereby whole tumor sections were scanned by hand using a Nikon Optiphot-2 microscope and x20 objective. Using an eye-piece graticule marked with 25 random points (Chalkley grid) and blinded to the experimental groups, the observer counted the number of points falling on necrotic tissue. This number, as a % of total points counted, equated to necrosis, as a % of the total sectional area. Tissue sections were scanned at high power using an Aperio slide

scanner (ScanScope, Aperio ePathology Solutions, Oxford, UK) for hypoxia analysis. Viable tumor regions were outlined and % hypoxia in viable regions calculated from the number of positive brown pixels and total pixels in viable regions, after setting suitable threshold levels (ImageScope software, Aperio ePathology Solutions, Oxford, UK).

Double immunofluorescent staining was performed on frozen 7-10 μm tumor sections, using the Pharmingen antibody above for CD31 and a mouse anti-mouse α-smooth muscle actin (α-SMA) monoclonal antibody (Cat no. A5228, Sigma-Aldrich, Poole, UK). Biotin-streptavidin technology was used to visualize signals, using Texas red and FITC (Vector Laboratories, Burlingame, CA, USA) to identify CD31 and α-SMA respectively. Tumor sections were viewed using a x10 objective on a Leica DMI 4000B advanced fluorescence microscope and images across the whole of each section captured for quantitation of fluorescence using in-house-developed software. Briefly, this consisted of thresholding for each fluorescence channel and calculating the amount of α-SMA staining as a % of the amount of CD31 staining for each tumor.

Phospho-receptor tyrosine kinase (RTK) analysis and western blotting

Analysis of RTK phosphorylation in extracts of frozen tumor samples was performed using a mouse phospho-RTK array kit (39 RTK receptors, R&D Systems, Abingdon, UK), following the manufacturer's instructions. Briefly, tumors were homogenized in ice cold PBS, with protease and phosphatase inhibitors, and microcentrifuged with 1% Triton X-100. Protein in supernatants was quantified using the Pierce BCA protein assay kit (Thermo Scientific, Cramlington, UK). Array membranes were incubated with 300 μg of protein overnight at 4^{o}C, washed and incubated with anti-

phosphotyrosine HRP detection antibody for 2 h at room temperature. After washing, arrays were incubated with ECL plus reagents (GE-Healthcare, Chalfont St Giles, UK) and exposed to X-ray film. Developed films were scanned on a Bio-Rad GS-710 densitometer (Bio-Rad Laboratories, Hemel Hempstead, UK) and the ratios of optical densities from SU5416-treated and vehicle-treated tumor samples calculated for assessment of the effect of treatment on each of the RTK phosphorylation levels.

Proteins extracted from tumors in the 6 h group were analysed for phosphorylated ERKs (pERK) by western blotting. Equal protein amounts (50-100 mg/lane) were separated on 7% NuPAGE Novex gels (Invitrogen, Life Technologies, Paisley, UK), transferred to PVDF membranes and probed overnight with an antibody to pERK (Cell Signaling Technology, New England Biolabs, Hitchin, UK). Membranes were washed and incubated with HRP-conjugated secondary antibodies (Dako, Ely UK) and immunoreactive bands were visualized using ELC plus reagents (GE Healthcare, Little Chalfont, UK). Blots were re-probed with an anti-GAPDH antibody (Cell Signaling Technology) and films were scanned as described above. pERK band densities were normalized to GAPDH.

Tumor interstitial fluid pressure

Tumors were treated with two doses of SU5416, as described above. Interstitial fluid pressure (IFP) was measured just prior to the first dose of SU5416 and 24 h after the second dose using the wick-in-needle technique [31]. Briefly, measurements were made using a 23G needle with side-port, connected to a pressure transducer (Model P23XL, Viggo-Spectramed, Windlesham, Surrey) via polyethylene tubing. The whole system was filled with heparinized saline and a nylon ‘wick’ was placed in the distal portion

of the needle to ensure direct contact with the tissue. Measurements were taken in at least three locations in each tumor and the average value was taken to represent the tumor IFP.

Intravital microscopy

Surgery for intravital microscopy was carried out on male SCID mice (12-16 week-old, 28-32g) under general anaesthesia with Hypnorm (fentanyl citrate and fluanisone; Janssen Animal Health) and Hypnovel (midazolam, Roche, Welwyn Garden City, UK), as described previously [32]. Briefly, an aluminium window chamber (total weight ~2g), designed to hold two parallel glass windows 200 μm apart to allow tumor growth, was implanted into a dorsal skin flap. A tumor fragment (~0.5 mm in diameter; tumor cells expressing VEGF120 or 188) from a donor animal was implanted onto the surgically exposed panniculus muscle of one skin layer and the chamber closed with a glass window. Following recovery from anaesthesia, animals were kept in a warm room, 28-30 $^{\circ}$C, until further experimentation. Animals received either SU5416 (50 mg/kg ip) or drug vehicle (DMSO 0.05 ml) starting at day 3 after implant and then every 3rd to 4th day until they reached ~ 3mm diameter (1 – 2 weeks after surgery), when they were treated with a single dose of CA4P (30 mg/kg iv at 3 mg/ml in 0.9% NaCl) or saline vehicle.

Intravital microscopy was carried out from day 1 after surgery and at various times after administration of CA4P up to 24 h. Transmitted light images were acquired using a Nikon Eclipse E600FN microscope. Vascular length was analysed from images captured with a x10 objective, using in-house developed software, as described previously [32]. Vascular length measurements were made in 2 selected regions of interest (ROIs) in each tumor. A single vessel was defined as a vessel

length between two branch-points. Red blood cell velocity (RCV) was also measured from the selected ROIs using a x20 microscope objective. For this, donor red blood cells, acquired via cardiac puncture from donor mice, were labelled with the fluorescent membrane marker, DiI (Molecular Probes, Cambridge Biosciences, UK), as described previously [33]. The labelled cells (0.1 - 0.2 ml in PBS) were administered to recipient animals via a tail vein cannula just prior to CA4P/vehicle administration – a single injection being sufficient to visualise the red cells for at least 24 h. 60 s video sequences under epi-fluorescence were captured, at 25 frames/s, using a Sony DSR-30P digital videocassette recorder, from which the full time-course of tumor RCV was calculated using an in-house-developed tracking algorithm [34]. Preliminary data for RCV effects of CA4P at a single time-point (24 h) after CA4P ± SU5416 have been published as conference proceedings [35]

Statistics

A one-way analysis of variance (ANOVA), followed by a Tukey Kramer hsd post-test was used for comparing multiple groups; a students unpaired t-test was used for comparing two independent groups; a paired t-test was used for comparing IFP before and after treatment in the same tumor; a 2-way ANOVA followed by a Bonferroni post-test was used for analyzing multiple groups with more than one variable (treatment and tumor type) (Prism 5 for Mac OS X). Differences between groups, where time-courses were obtained, were analysed using a mixed design ANOVA for repeated measures (SPSS version 11.0.2, for the Apple Macintosh, SPSS Inc). In all cases, differences between groups were described as significant if the probability corresponding to the appropriate statistic was < 0.05.

Results

Tumor vascular effects of chronic treatment with SU5416

Figure 1 shows the effects of SU5416 on vascular morphology in sub-cutaneous tumors at 24 and 48h after two doses of SU5416. SU5416 caused a significant reduction in CD31+ vascular area and vascular density per viable field (Figure 1A & B). The decreases observed were moderate and did not reach statistical significance for individual pairs of data (Figure 1A). The highly dense networks of small calibre vessels in the VEGF188 tumors (Figure 1A and B) have been reported previously [17]. Morphometric analysis of the shape of individual vessels revealed no effects of SU5416 in either tumor type (data not shown). However, it was noted qualitatively that CD31 staining, especially in VEGF120 tumors, partially filled the lumen of larger vessels in vehicle-treated tumors, whereas this was less apparent in SU5416-treated tumors, as shown in Figure 1B. These larger vessels were more common in VEGF120 than in VEGF188 tumors and in SU5416-treated compared with vehicle-treated tumors (Figure 1B). In a different sub-set of vessels, SU5416-induced vascular damage was clearly apparent, as evidenced by regions of tumor cell necrosis surrounding isolated small blood vessels (Figure 1C).

Maturity of the tumor vascular wall was determined quantitatively by measuring the extent of α-SMA staining relative to that of CD31, using immunofluorescence in frozen tumor sections. VEGF188-expressing tumors expressed significantly higher relative levels of α-SMA staining than VEGF120-expressing tumors (Figure 1D), indicative of greater vascular maturity, as previously reported [17]. There was no effect of SU5416 treatment on vascular maturity, as measured by α-SMA staining, in either tumor type (Figure 1D).

Effects of SU5416 on sub-cutaneous tumors were insufficient to cause any slowing of tumor growth or necrosis induction (Figure 2A & B). However, there was a differential effect of the drug on IFP in the two tumor types. Figure 2C shows that IFP was higher in untreated VEGF120 than in VEGF188 tumors. IFP in VEGF120 tumors increased further with time, in the vehicle-treated group, which was suppressed by SU5416 treatment, whereas SU5416 treatment had no effect on IFP in VEGF188 tumors (Figure 2C).

SU5416 treatment caused moderate suppression of phosphorylation of various receptor tyrosine kinases (RTKs), including VEGFR-2 and other known targets of the drug such as SCF R, Flt3, c-RET and PDGFR-β, as well as other RTKs, in both VEGF120- and VEGF188-expressing tumors for at least 48 h (Figure 2D and Supplementary Figure 1). We were unable to detect phosphorylated VEGFR-2 by western blotting of tumor extracts (data not shown). However, pERK was detectable and results for tumors excised at 6h are shown in Figure 2D. The protein array and western blotting analyses provide only semi-quantitative results that are not amenable to rigorous statistical analysis. However, taken together with the vascular morphology results (Figure 1), they indicate tumor activity of SU5416 in our systems. There is an indication that SU5416 was more effective in suppressing RTK phosphorylation in VEGF120 than in VEGF188 tumors (Figure 2D), however this would need further investigation to clarify.

Figure 3 shows the effects of SU5416 on vascular morphology and function of tumors growing in window chambers. Figure 3A shows representative images of the tumor vasculature at the end of SU5416 or vehicle treatment. Figure 3B shows that there was significant vascular loss in VEGF188-expressing tumors following SU5416 treatment. The situation for VEGF120 tumors was more complex, with no

overall vascular loss (Figure 3B) but a tendency for rarefaction of the densely vascularised tumor border following SU5416 treatment (Figure 3A). Vascular loss in VEGF188 tumors was accompanied by an increase in the average length of individual vessels (Figure 3B), suggesting a 'pruning' effect of the drug on the smaller vascular branches. Interestingly, prior to treatment, red cell velocity (RCV) was higher in VEGF188-expressing tumors than in control VEGF120-expressing tumors (372 ± 82 μm/s and 188 ± 28 μm/s respectively). Most notably, SU5416 treatment resulted in a significant increase in RCV in VEGF120 tumors, whereas there was no effect in VEGF188 tumors, so that RCV was equalised in the two tumor types after treatment (Figure 3C).

Considering both sub-cutaneous and window chamber tumors, there was overall evidence for a small anti-vascular effect of SU5416 in both VEGF120- and VEGF188-expressing tumors. In contrast, SU5416 had no effect on vascular function in VEGF188 tumors (assessed by measurement of RCV), whereas vascular function in VEGF120 tumors was normalised to the level found in vehicle-treated VEGF188 tumors.

Effect of SU5416 pre-treatment on response to the vascular disrupting agent CA4P

Typical low power images of tumors growing in dorsal skin-fold window chambers, at various times following a single dose of CA4P, are shown in Figure 4. Quantitative analyses of the effects of CA4P on visible vascular length and RCV are shown in Figure 5; these data were derived from two high power regions from each tumor as illustrated in Figure 4. Taken together, data in Figures 4 and 5 show a moderate decrease in the visible vascular length up to 1 hour after CA4P, which recovers to different extents by 3 hours. In VEGF120 tumors that did not receive

SU5416, this recovery was un-sustained and these tumors became highly avascular by 24 hours after CA4P, indicative of necrosis (Figures 4 and 5), which was typically accompanied by a severe hemorrhagic episode at approximately 6 hours (Figure 4). In VEGF188 tumors, there was a smaller decrease in visible vascular length within the first hour of CA4P treatment (not falling below 70% of pre-treatment levels), which was followed by partial recovery to approximately 85% of pre-treatment levels, sustained for the full 24-hour observation period. RCV decreased very rapidly in VEGF120 tumors reaching a minimum of less than 20% of the pre-treatment level by 3 hours, with no recovery by 24 hours. As for vascular length, CA4P had less effect on RCV in VEGF188 tumors (Figures 4 and 5), with complete recovery of velocity by 24 hours after treatment. A relative resistance of VEGF188 tumors to CA4P compared with VEGF120 tumors is consistent with our previous findings [17]. However, the most striking effect was that pre-treatment with SU5416 protected sensitive VEGF120 tumors from the damaging effects of CA4P. In this case, both vascular length and red blood cell velocity recovered to near pre-treatment levels by 24 hours (Figure 5) and the development of hemorrhage at 6 hours and avascular areas at 24 hours were completely abrogated by SU5416 pre-treatment (Figure 4). Some protection from the effects of CA4P by SU5416 pre-treatment was also observed in VEGF188 tumors, although this was less profound due to their innate resistance to the drug (Figure 5).

Effects of SU5416 pre-treatment on vascular response of s.c. tumors to CA4P were also studied. Figure 6A shows quantitation of CD31 staining at 3 h after CA4P administration ± SU5416 pre-treatment. Surprisingly, CA4P treatment tended to increase CD31 staining compared with vehicle-treated tumors, which was significantly abrogated by SU5416 pre-treatment in VEGF120 but not VEGF188

tumors. Examination of staining patterns (Figure 6B) showed that there was extensive vascular damage in CA4P-treated tumors. In particular, endothelial layers were severely fragmented (Figure 6Bii) and iii) compared with i) and viii) compared with vii)). There were many large, distended vessels stacked with red blood cells, especially towards the centre of VEGF120 tumors (Figure 6Biii)). Fragmentation of vessels caused the algorithm to identify several 'objects' per vessel in the CA4P-treated groups, as indicated by the yellow arrows in Figure 6Biv). Disrupted endothelial cells also resulted in CD31 staining spreading into vessel lumens (Figure 6Bii)). These two effects explain the quantified data in Figure 6A. SU5416 pre-treatment partially blocked the damaging effects of CA4P on vascular morphology in both tumor types (Figure 6Bv), vi), viii) and ix)), although this was only statistically significant in VEGF120 tumors (Figure 6A).

Pimonidazole adduct staining indicated approximately 60% hypoxia in viable regions of both untreated VEGF120 and VEGF188 tumors, which was unaffected by SU5416 treatment (Supplementary Figure 2A and B). CA4P treatment caused increased staining of peripheral tumor regions but a decrease in staining in tumor centres, which was significant for VEGF188 tumors (Supplementary Figure 2A). These tumor regions suffered extreme vascular damage from CA4P (Figure 6) and it is likely that pimonidazole could not access them. Supplementary Figure 2C shows severely damaged central vessels with red cells haemorrhaging into the surrounding tissue. Pimonidazole adduct staining in CA4P-treated tumors that had been pre-treated with SU5416 was equivalent to that in vehicle-treated tumors. Although not conclusive in their own right, these results are consistent with the protective effect of SU5416 against CA4P treatment shown in Figures 4, 5 and 6.

Discussion

We have shown that mouse fibrosarcoma cells, which express only single isoforms of VEGF, produce solid tumors with different susceptibilities to two diverse therapeutic strategies for targeting tumor blood vessels. Specifically, VEGF120-expressing tumors, which have fragile blood vessels that are poorly invested with pericytes, responded avidly to an acute treatment with the vascular disrupting agent, CA4P. These tumors suffered only a minor vascular loss following chronic treatment with the anti-angiogenic agent, SU5416, with no significant effect in window chamber preparations. However, the vasculature showed distinct signs of normalization (increase in RCV in window chamber preparations and modulation of IFP in s.c. tumors). VEGF188-expressing tumors, which have a higher vascular density and red cell velocity and greater pericyte coverage than VEGF120-expressing tumors in the unperturbed state, were able to recover more effectively than VEGF120 tumors from the initial vascular-damaging effects of CA4P (window chamber results). The anti-angiogenic effects of SU5416 were also only moderate in VEGF188 tumors but there were no gross signs of vascular normalization in this tumor type. Most notably, SU5416-induced vascular normalization in VEGF120 tumors was associated with an acquired resistance to CA4P, such that they responded more like untreated VEGF188 tumors in the window chamber assay. In contrast, SU5416 had no effect on red blood cell velocity in VEGF188 tumors, although response to CA4P was still moderately reduced by pre-treatment with SU5416. Overall our results suggest that tumors expressing high levels of VEGF120 are particularly susceptible to vascular normalization but that this process renders them insensitive to subsequent vascular disrupting approaches.

SU5416 was previously shown to elicit both a reduction in vascular density and vascular normalization in a rat glioma model transplanted into nude mice [13] and in a hamster melanoma model [14]. A reduction in tumor growth rate was also observed in both these studies. In contrast, Ansiaux *et al.* [36] reported an absence of vascular re-modeling and growth retardation in a transplanted liver tumor and fibrosarcoma mouse model in response to SU5416 treatment, illustrating variability in response to this agent between different tumor types. A daily dosing strategy was employed in all these studies. In the current study, we used an intermittent dosing strategy, consistent with that used clinically and based on evidence that a twice-weekly dosing strategy was as efficacious as a daily dosing strategy, in the A357 human melanoma tumor model [37]. Prolonged biological activity for several days is due to sequestration of this hydrophobic drug in lipid membranes [38]. Clinical trials with SU5416 were unsuccessful, with no or minimal decrease in microvascular density in advanced cancers of mixed origin and inflammatory breast cancer [39, 40]. In our mouse fibrosarcomas, we also showed only moderate anti-angiogenic effects of SU5416, intermediate between those observed in the above pre-clinical studies, with no growth retardation in either tumor type. Window chamber experiments indicated that there was a greater effect of SU5416 in the periphery than in the centre of VEGF120 tumors, which is consistent with observations in other tumor types [41]. In subcutaneously implanted tumors, these effects were consistent with only a small inhibition of VEGFR-2 phosphorylation in both VEGF120 and VEGF188 tumors. RTK phosphorylation profiling of tumor samples also showed inhibition of other known and less well-known targets of SU5416, which is likely to have contributed to the vascular effects observed.

Vascular normalization was more apparent in VEGF120 tumors than VEGF188 tumors, as exemplified by the increase in red blood cell velocity in the former but not the latter tumor type. Normalization is a complex process that can occur following a range of treatment modalities [42]. Indeed, it was first identified in the 1970s by Le Serve and Hellman [43] following treatment with the anti-metastatic drug razoxane, although it is most commonly associated with anti-angiogenic drugs [5]. Although the molecular control mechanisms are poorly understood, morphological features can include a moderate reduction in microvascular density, change in vessel diameter and improved pericyte coverage, which may lead to an increase in blood flow, reduced vascular permeability and/or improved oxygenation [5]. In VEGF120 tumors the increase in red blood cell velocity was not associated with any detectable increase in pericyte coverage. This may be due to the known inhibitory effect of SU5416 on PDGFR-β, which was also demonstrated in the current study. On examination of tumor sections stained for CD31, we commonly observed CD31+ cells bridging the lumen of the larger vessels in VEGF120 tumors but less commonly so in VEGF188 tumors. VEGF120 lacks the C-terminal heparin-binding motifs of the larger isoforms and its consequent diffusibility is thought to account for misguidance of endothelial cell migration [44], which could explain our observation. These endothelial cell 'bridges' were reduced and wider caliber open vessels were more evident following SU5416 treatment. These effects could at least partially explain the increase in red cell velocity observed. In addition, we found higher interstitial fluid pressure (IFP) in VEGF120 compared with VEGF188 tumors, which is most likely related to our previous finding of highly permeable vessel walls in the former [17]. SU5416 pre-treatment affected IFP differently in the two tumor types, preventing the increase in IFP that was observed over time in VEGF120 tumors. SU5416 also

prevented the characteristic hemorrhagic response of VEGF120 tumors to CA4P in window chambers, indicating a reduction in vascular permeability. A reduction in IFP has previously been proposed as a driver for tumor vascular normalization, possibly via oedema reduction [13].

SU5416-induced vascular normalization resulted in VEGF120 tumors acquiring resistance to subsequent treatment with CA4P. This effect was substantial, with a complete abrogation of the hemorrhagic response in window chambers, at approximately 6 h after treatment, and abrogation of the subsequent loss of vascularity by 24 hours. Various features of vascular normalization could account for this effect. Firstly, CA4P causes a very rapid decrease in blood flow to tumors, within minutes of treatment, as shown in the current study. The SU5416-induced increase in red cell velocity in VEGF120 tumors may therefore have protected the tumors against blood flow dropping to levels that cause ischemic damage in response to CA4P. In addition, fragility of the vascular walls in VEGF120 tumors makes them particularly susceptible to damage by CA4P, resulting in an increase in vascular permeability, hemorrhage and tumor necrosis [17]. Prevention of the hemorrhagic response to CA4P by SU5416 pre-treatment suggests that SU5146 reversed the well-known influence of VEGF on vascular permeability. This effect would not have been so apparent in VEGF188 tumors, where we have shown vessels to be less permeable and less prone to hemorrhage than in VEGF120 tumors [17]. Although SU5416 had the greatest impact on response to normally CA4P-sensitive VEGF120 tumors, there was also a significant SU5416-induced reduction in response to CA4P in VEGF188 tumors, as seen in s.c., as well as window chamber tumors. This suggests that the decrease in vascularity associated with SU5416 treatment in this tumor type did cause some hemodynamic changes that were not detected with the assays used in these

investigations. Nevertheless, it is clear that by far the greatest effects on response to CA4P were found in VEGF120 tumors.

Advances in cancer therapy rely to a large extent on understanding the mechanisms and consequences of combining targeted treatments, including vascular-targeted treatments, with each other as well as with conventional therapy. VDAs represent a promising group of novel compounds for tumor vascular targeting but the severe tumor hypoxia that accompanies ischemia raises the concern that re-growing tumors from surviving cells will be particularly aggressive [45]. In addition, VDAs have been shown to increase the number of circulating endothelial progenitor cells and tumor-infiltrating macrophages after treatment, processes that can contribute to tumor re-vascularization [46, 47]. Consistent with these considerations, several pre-clinical studies have shown that combining VDAs with a subsequent anti-angiogenic treatment such as neutralising antibodies for VEGF (bevacizumab) or VEGFR-2 (DC101) or a receptor tyrosine kinase inhibitor increases the tumor regrowth delay found for either agent alone [48-50]. Our study sounds a note of caution, suggesting that, if vascular normalization occurs following anti-angiogenic treatment, this would reduce the efficacy of a subsequent VDA treatment.

In conclusion, although vascular normalization can increase the delivery of chemotherapeutic drugs to tumor tissue, it can also reduce the efficacy of VDA treatment. Predictive bio-markers are urgently required for personalized cancer treatments. We have shown that expression of individual isoforms of VEGF can influence susceptibility of tumor vasculature to the normalization process and therefore may be useful for predicting response to anti-angiogenic, as well as vascular-disrupting, therapy.

Acknowledgements

This work was funded by a programme grant from Cancer Research UK (C1276/A9993). We would like to thank Dr Joanne Bluff for her help with immunohistochemistry and microscopy and Professor Bob Pettit for supply of CA4P. We also thank Dr Jamila Ibrahim for reading an early draft of this manuscript and staff at the University of Sheffield for care of the animals.

References

1. Ellis LM, Hicklin DJ. VEGF-targeted therapy: mechanisms of anti-tumor activity. Nat Rev Cancer 2008;8:579-91.
2. Tugues S, Koch S, Gualandi L, Li X, Claesson-Welsh L. Vascular endothelial growth factors and receptors: anti-angiogenic therapy in the treatment of cancer. Mol Aspects Med 2011;32:88-111.
3. Ferrara N. Vascular endothelial growth factor: basic science and clinical progress. Endocr Rev 2004;25:581-611.
4. Carmeliet P, Jain RK. Principles and mechanisms of vessel normalization for cancer and other angiogenic diseases. Nat Rev Drug Discov 2011;10:417-27.
5. Goel S, Duda DG, Xu L, Munn LL, Boucher Y, Fukumura D, Jain RK. Normalization of the vasculature for treatment of cancer and other diseases. Physiol Rev 2011;91:1071-121.
6. Willett CG, Boucher Y, di Tomaso E, Duda DG, Munn LL, Tong RT, Chung DC, Sahani DV, Kalva SP, Kozin SV, Mino M, Cohen KS, et al. Direct evidence that the VEGF-specific antibody bevacizumab has antivascular effects in human rectal cancer. Nat Med 2004;10:145-7.

7. Batchelor TT, Sorensen AG, di Tomaso E, Zhang WT, Duda DG, Cohen KS, Kozak KR, Cahill DP, Chen PJ, Zhu M, Ancukiewicz M, Mrugala MM, et al. AZD2171, a pan-VEGF receptor tyrosine kinase inhibitor, normalizes tumor vasculature and alleviates edema in glioblastoma patients. Cancer Cell 2007;11:83-95.

8. Fong TA, Shawver LK, Sun L, Tang C, App H, Powell TJ, Kim YH, Schreck R, Wang X, Risau W, Ullrich A, Hirth KP, et al. SU5416 is a potent and selective inhibitor of the vascular endothelial growth factor receptor (Flk-1/KDR) that inhibits tyrosine kinase catalysis, tumor vascularization, and growth of multiple tumor types. Cancer Res 1999;59:99-106.

9. Krystal GW, Honsawek S, Kiewlich D, Liang C, Vasile S, Sun L, McMahon G, Lipson KE. Indolinone tyrosine kinase inhibitors block Kit activation and growth of small cell lung cancer cells. Cancer Res 2001;61:3660-8.

10. Yee KW, O'Farrell AM, Smolich BD, Cherrington JM, McMahon G, Wait CL, McGreevey LS, Griffith DJ, Heinrich MC. SU5416 and SU5614 inhibit kinase activity of wild-type and mutant FLT3 receptor tyrosine kinase. Blood 2002;100:2941-9.

11. Wang SY, Chen B, Zhan YQ, Xu WX, Li CY, Yang RF, Zheng H, Yue PB, Larsen SH, Sun HB, Yang X. SU5416 is a potent inhibitor of hepatocyte growth factor receptor (c-Met) and blocks HGF-induced invasiveness of human HepG2 hepatoma cells. J Hepatol 2004;41:267-73.

12. Latham AM, Bruns AF, Kankanala J, Johnson AP, Fishwick CW, Homer-Vanniasinkam S, Ponnambalam S. Indolinones and anilinophthalazines differentially target VEGF-A and bFGF-mediated responses in primary human endothelial cells. Br J Pharmacol 2012;16:245-59.

13. Vajkoczy P, Menger MD, Vollmar B, Schiling L, Schmiedek P, Hirth KP, Ullrich A, Fong TAT. Inhibition of tumor growth angiogenesis and microcirculation by the novel Flk-1 inhibitor SU5416 as assessed by intravital multi-'fluorescence videomicroscopy. Neoplasia 1999;1:31-41.

14. Eichhorn ME, Strieth S, Luedemann S, Kleespies A, Noth U, Passon A, Brix G, Jauch KW, Bruns CJ, Dellian M. Contrast enhanced MRI and intravital fluorescence microscopy indicate improved tumor microcirculation in highly vascularized melanomas upon short-term anti-VEGFR treatment. Cancer Biol Ther 2008;7:1006-13.

15. Ruhrberg C, Gerhardt H, Golding M, Watson R, Ioannidou S, Fujisawa H, Betsholtz C, Shima DT. Spatially restricted patterning cues provided by heparin-binding VEGF-A control blood vessel branching morphogenesis. Genes Dev 2002;16:2684-98.

16. Grunstein J, Masbad JJ, Hickey R, Giordano F, Johnson RS. Isoforms of vascular endothelial growth factor act in a coordinate fashion to recruit and expand tumor vasculature. Mol Cell Biol 2000;20:7282-91.

17. Tozer GM, Akerman S, Cross NA, Barber PR, Bjorndahl MA, Greco O, Harris S, Hill SA, Honess DJ, Ireson CR, Pettyjohn KL, Prise VE, et al. Blood vessel maturation and response to vascular-disrupting therapy in single vascular endothelial growth factor-A isoform-producing tumors. Cancer Res 2008;68:2301-11.

18. Shima DT, Kuroki M, Deutsch U, Ng YS, Adamis AP, D'Amore PA. The mouse gene for vascular endothelial growth factor. Genomic structure, definition of the transcriptional unit, and characterization of transcriptional and post-transcriptional regulatory sequences. J Biol Chem 1996;271:3877-83.

19. Ferrara N, Gerber H-P, LeCouter J. The biology of VEGF and its receptors. Nat Med 2003;9:669-76.

20. Stimpfl M, Tong D, Fasching B, Schuster E, Obermair A, Leodolter S, Zeillinger R. Vascular endothelial growth factor splice variants and their prognostic value in breast and ovarian cancer. Clin Cancer Res 2002;8:2253-9.

21. Yu JL, Rak JW, Klement G, Kerbel RS. Vascular endothelial growth factor isoform expression as a determinant of blood vessel patterning in human melanoma xenografts. Cancer Res 2002;62:1838-46.

22. Tokunaga T, Oshika Y, Abe Y, Ozeki Y, Sadahiro S, Kijima H, Tsuchida T, Yamazaki H, Ueyama Y, Tamaoki N, Nakamura M. Vascular endothelial growth factor (VEGF) mRNA isoform expression pattern is correlated with liver metastasis and poor prognosis in colon cancer. Br J Cancer 1998;77:998-1002.

23. Tomisawa M, Tokunaga T, Oshika Y, Tsuchida T, Fukushima Y, Sato H, Kijima H, Yamazaki H, Ueyama Y, Tamaoki N, Nakamura M. Expression pattern of vascular endothelial growth factor isoform is closely correlated with tumour stage and vascularisation in renal cell carcinoma. Eur J Cancer 1999;35:133-7.

24. Yuan A, Yu CJ, Kuo SH, Chen WJ, Lin FY, Luh KT, Yang PC, Lee YC. Vascular endothelial growth factor 189 mRNA isoform expression specifically correlates with tumor angiogenesis, patient survival, and postoperative relapse in non-small-cell lung cancer. J Clin Oncol 2001;19:432-41.

25. O-charoenrat P, Rhys-Evans P, Eccles SA. Expression of vascular endothelial growth factor family members in head and neck squamous cell carcinoma correlates with lymph node metastasis. Cancer 2001;92:556-68.

26. Gorski DH, Leal AD, Goydos JS. Differential expression of vascular endothelial growth factor-A isoforms at different stages of melanoma progression. J Am Coll Surg 2003;197:408-18.

27. Chen TT, Luque A, Lee S, Anderson SM, Segura T, Iruela-Arispe ML. Anchorage of VEGF to the extracellular matrix conveys differential signaling responses to endothelial cells. J Cell Biol 2010;188:595-609.

28. Workman P, Aboagye EO, Balkwill F, Balmain A, Bruder G, Chaplin DJ, Double JA, Everitt J, Farningham DA, Glennie MJ, Kelland LR, Robinson V, et al. Guidelines for the welfare and use of animals in cancer research. Br J Cancer 2010;102:1555-77.

29. Raleigh JA, Calkins-Adams DP, Rinker LH, Ballenger CA, Weissler MC, Fowler WC, Novotny DB, Varia MA. Hypoxia and vascular endothelial growth factor expression in human squamous cell carcinomas using pimonidazole as a hypoxia marker. Cancer Research 1998;58:3765-8.

30. Reyes-Aldasoro CC, Williams LJ, Akerman S, Kanthou C, Tozer GM. An automatic algorithm for the segmentation and morphological analysis of microvessels in immunostained histological tumour sections. J Microsc 2011;242:262-78.

31. Lunt SJ, Kalliomaki TM, Brown A, Yang VX, Milosevic M, Hill RP. Interstitial fluid pressure, vascularity and metastasis in ectopic, orthotopic and spontaneous tumours. BMC Cancer 2008;8:2.

32. Tozer GM, Ameer-Beg SM, Baker J, Barber PR, Hill SA, Hodgkiss RJ, Locke R, Prise VE, Wilson I, Vojnovic B. Intravital imaging of tumour vascular networks using multi-photon fluorescence microscopy. Adv Drug Deliv Rev 2005;57:135-52.

33. Tozer GM, Prise VE, Wilson J, Cemazar M, Shan S, Dewhirst MW, Barber PR, Vojnovic B, Chaplin DJ. Mechanisms associated with tumor vascular shut-down induced by combretastatin A-4 phosphate: intravital microscopy and measurement of vascular permeability. Cancer Res 2001;61:6413-22.

34. Reyes-Aldasoro CC, Akerman S, Tozer GM. Measuring the velocity of fluorescently labelled red blood cells with a keyhole tracking algorithm. J Microsc 2008;229:162-73.

35. Akerman S, Reyes-Aldasoro CC, Fisher M, Pettyjohn KL, Bjorndahl MA, Evans H, Tozer GM. Microflow of fluorescently labelled red blood cells in tumours expressing single isoforms of VEGF and their response to vascular targeting agents. Med Eng Phys 2011;33:805-9.

36. Ansiaux R, Baudelet C, Jordan BF, Crokart N, Martinive P, DeWever J, Gregoire V, Feron O, Gallez B. Mechanism of reoxygenation after antiangiogenic therapy using SU5416 and its importance for guiding combined antitumor therapy. Cancer Res 2006;66:9698-704.

37. Mendel DB, Laird AD, Smolich BD, Blake RA, Liang C, Hannah AL, Shaheen RM, Ellis LM, Weitman S, Shawver LK, Cherrington JM. Development of SU5416, a selective small molecule inhibitor of VEGF receptor tyrosine kinase activity, as an anti-angiogenesis agent. Anticancer Drug Des 2000;15:29-41.

38. Mendel DB, Schreck RE, West DC, Li G, Strawn LM, Tanciongco SS, Vasile S, Shawver LK, Cherrington JM. The angiogenesis inhibitor SU5416 has long-lasting effects on vascular endothelial growth factor receptor phosphorylation and function. Clin Cancer Res 2000;6:4848-58.

39. Dowlati A, Robertson K, Radivoyevitch T, Waas J, Ziats NP, Hartman P, Abdul-Karim FW, Wasman JK, Jesberger J, Lewin J, McCrae K, Ivy P, et al. Novel Phase I dose de-escalation design trial to determine the biological modulatory dose of the antiangiogenic agent SU5416. Clin Cancer Res 2005;11:7938-44.

40. Overmoyer B, Fu P, Hoppel C, Radivoyevitch T, Shenk R, Persons M, Silverman P, Robertson K, Ziats NP, Wasman JK, Abdul-Karim FW, Jesberger JA, et al. Inflammatory breast cancer as a model disease to study tumor angiogenesis: results of a phase IB trial of combination SU5416 and doxorubicin. Clin Cancer Res 2007;13:5862-8.

41. Vajkoczy P, Thurnher A, Hirth KP, Schilling L, Schmiedek P, Ullrich A, Menger MD. Measuring VEGF-Flk-1 activity and consequences of VEGF-Flk-1 targeting in vivo using intravital microscopy: clinical applications. Oncologist 2000;5:16-9.

42. Qayum N, Muschel RJ, Im JH, Balathasan L, Koch CJ, Patel S, McKenna WG, Bernhard EJ. Tumor vascular changes mediated by inhibition of oncogenic signaling. Cancer Res 2009;69:6347-54.

43. Le Serve AW, Hellmann K. Metastases and the normalization of tumour blood vessels by ICRF 159: a new type of drug action. Br Med J 1972;1:597-601.

44. Lundkvist A, Lee S, Iruela-Arispe L, Betsholtz C, Gerhardt H. Growth factor gradients in vascular patterning. Novartis Found Symp 2007;283:194-201; discussion -6, 38-41.

45. Tozer GM, Kanthou C, Lewis G, Prise VE, Vojnovic B, Hill SA. Tumour vascular disrupting agents: combating treatment resistance. Br J Radiol 2008;81 Spec No 1:S12-20.

46. Shaked Y, Tang T, Woloszynek J, Daenen LG, Man S, Xu P, Cai SR, Arbeit JM, Voest EE, Chaplin DJ, Smythe J, Harris A, et al. Contribution of granulocyte colony-stimulating factor to the acute mobilization of endothelial precursor cells by vascular disrupting agents. Cancer Res 2009;69:7524-8.

47. Welford AF, Biziato D, Coffelt SB, Nucera S, Fisher M, Pucci F, Di Serio C, Naldini L, De Palma M, Tozer GM, Lewis CE. TIE2-expressing macrophages limit the therapeutic efficacy of the vascular-disrupting agent combretastatin A4 phosphate in mice. Journal Clinical Invest 2011;121:1969-73.

48. Siemann DW, Shi W. Dual targeting of tumor vasculature: combining Avastin and vascular disrupting agents (CA4P or OXi4503). Anticancer Res 2008;28:2027-31.

49. Shaked Y, Ciarrocchi A, Franco M, Lee CR, Man S, Cheung AM, Hicklin DJ, Chaplin D, Foster FS, Benezra R, Kerbel RS. Therapy-induced acute recruitment of circulating endothelial progenitor cells to tumors. Science 2006;313:1785-7.

50. Shi W, Siemann DW. Targeting the tumor vasculature: enhancing antitumor efficacy through combination treatment with ZD6126 and ZD6474. In Vivo 2005;19:1045-50.

Figures

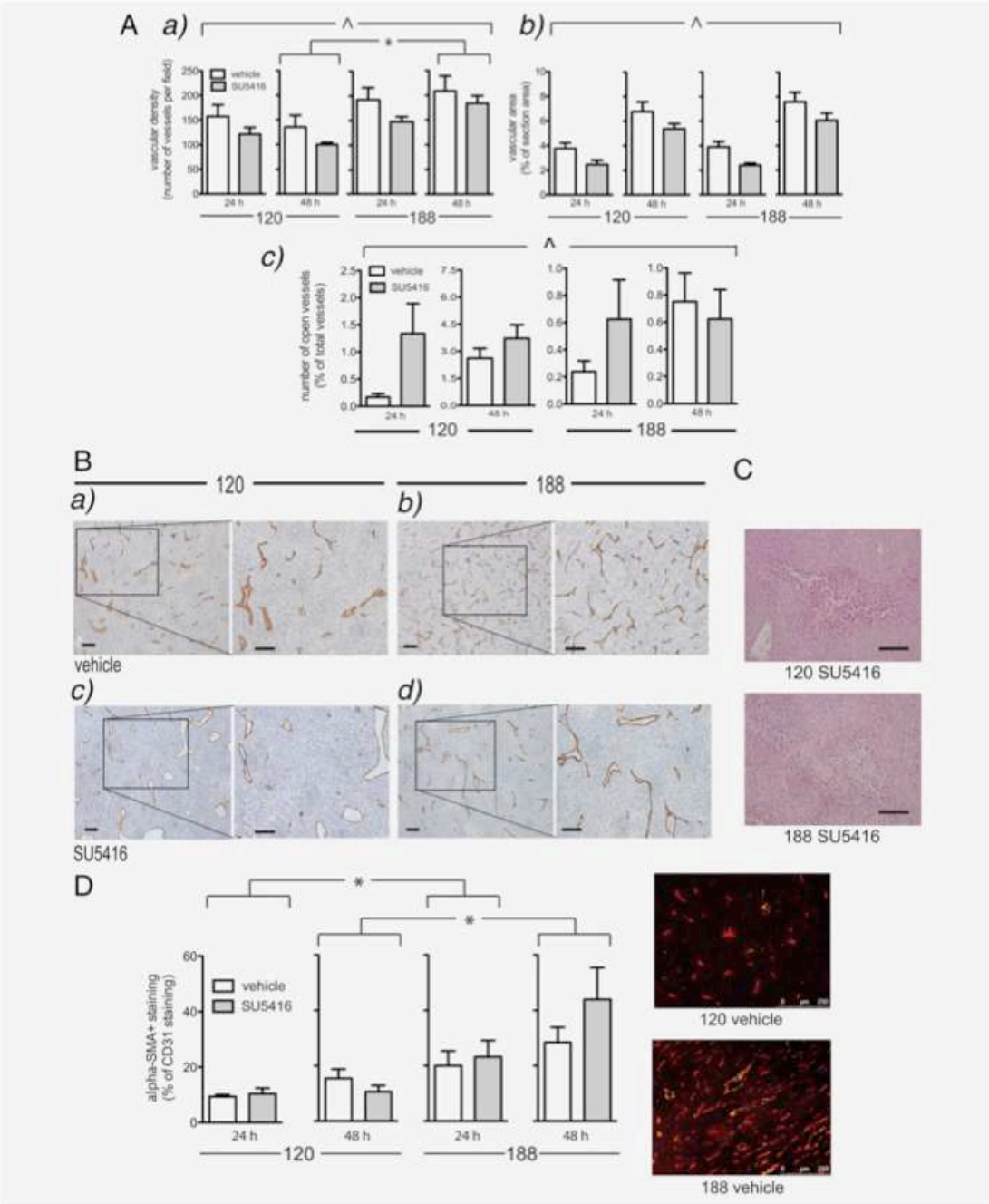

Figure 1

Effect of SU5416 on vascular morphology in sub-cutaneous VEGF120- and VEGF188-expressing tumors analysed at 24 or 48 h after the last dose of SU5416 or vehicle; see main text for dosing schedule. (A): Vascular density (number of vessels per field as defined by CD31 staining) and vascular area (% pixels positive for CD31)

in fixed tissue; n = 5-9 tumors per group; ≥ 7 high power ROIs per tumor; values are means ± 1 SEM. * represents a significant difference in vascular density between VEGF120- and VEGF188-expressing tumors. ^ represents an overall decrease in vascular density and vascular area with SU5416 treatment (2-way ANOVA with Bonferroni post-test; $P < 0.05$). There were no significant differences between individual pairs of data. (B): Examples of CD31 staining in fixed sections from tumors following vehicle or SU5416 treatment at different magnifications; i) and iv): vessels presented as narrow bands in untreated tumors, with isolated regions of large dilated vessels in SU5416-treated tumors (x10 objective) - individual vessels were commonly larger in VEGF-120 than in VEGF188 tumors. ii), iii), v) and vi): arrows represent endothelial cell 'bridges' in untreated tumors; rectangular regions in ii) and v) (x20 objective) are shown at higher power (x40 objective) in iii) and vi); scale bars are 100 μm. (C): Images from H&E stained sections of tumors treated with SU5416 showing isolated regions of necrosis surrounding blood vessels (x40 objective). (D): Graph shows extent of α-SMA+ staining relative to extent of CD31+ staining in frozen tumor sections; n = 5-9 tumors per group; ≥ 5 ROIs (x10 objective) per tumor; values are means ± 1 SEM. Images show examples of double immunofluorescence staining for CD31 (red) and α-SMA (yellow-orange) for vehicle-treated tumors. * represents a significant difference in staining ratio between VEGF120- and VEGF188-expressing tumors (2-way ANOVA with Bonferroni post-test; $P < 0.05$). Scale bars are 250 μm.

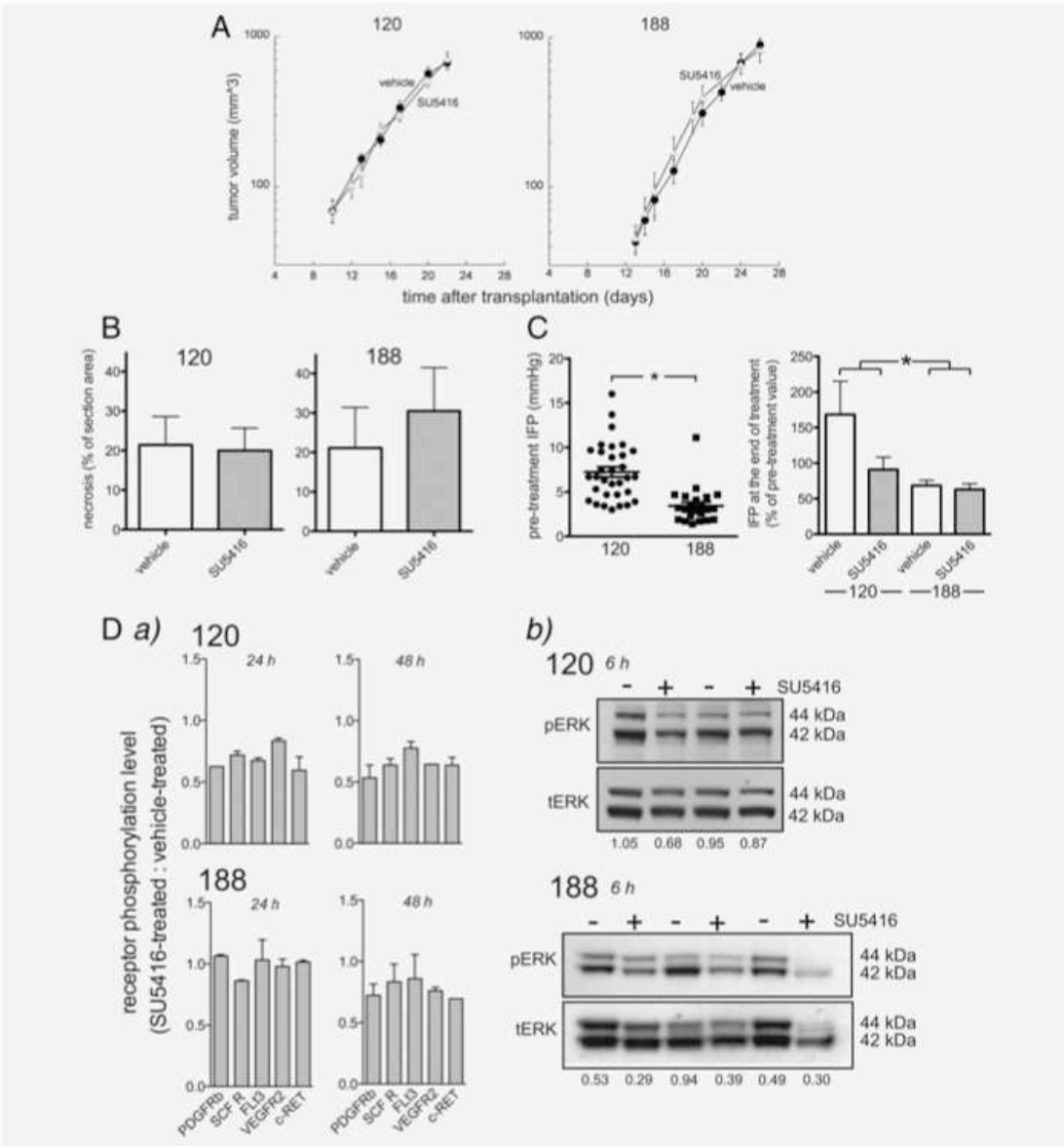

Figure 2

Effect of SU5416 on growth (A), % necrosis (B), interstitial fluid pressure (C) and receptor tyrosine kinase (RTK) phosphorylation (D) of VEGF120- and VEGF188-expressing sub-cutaneous tumors; see main text for dosing schedule. Data are means ± 1 SEM; n = 5-7 tumors per group in (A) and (B). At least 1000 random points per tumor were counted for necrosis calculation in (B) (see main text for details). The left-hand graph in (C) shows IFP for individual tumors and the mean ± 1 SEM prior to treatment. * represents a significant difference ($P < 0.05$; unpaired students t-test). The right-hand graph shows the effect of SU5416 in tumors, where IFP was obtained

before and after treatment in the same animal. Data are means ± 1 SEM for n = 8-14. * represents a significant difference in response of IFP to SU5416 between VEGF120- and VEGF188-expressing tumors (2-way ANOVA with Bonferroni post-test). (D): i) shows the X-ray film optical densities derived from exposure of phospho-RTK detection array membranes, following incubation with protein from tumor extracts. Results are expressed as the ratio of optical densities for tumors from animals treated with SU5416 versus those treated with vehicle. Each bar represents mean ±1 SEM for 3-4 tumors. Tumors were excised 24 or 48 h after the last dose of SU5416 or vehicle. The 5 known SU5416 targets of 39 RTK receptors are shown: platelet-derived growth factor receptor beta (PDGFRb); stem cell factor receptor/c-Kit (SCF-R); fms-like tyrosine kinase 3 (Flt3); VEGF receptor 2 (VEGFR2); c-RET receptor tyrosine kinase (c-RET). ii) shows western blots and resulting X-ray film optical densities for pERKs from tumor extracts for SU5416 or vehicle treatment at 6 h after the last dose of SU5416 or vehicle. Each bar represents mean ± 1 SEM for 3-4 tumors.

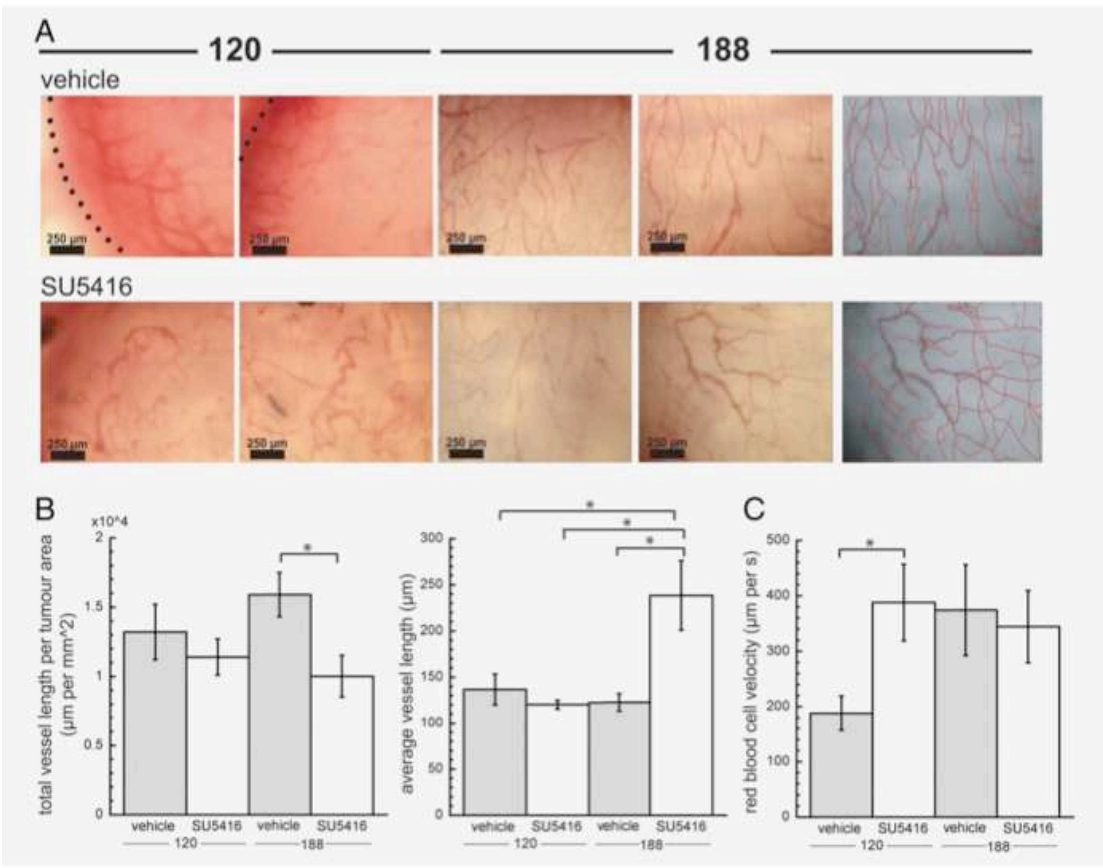

Figure 3

Effect of SU5416 on vascular morphology and function in VEGF120- and VEGF188-expressing tumors growing in dorsal skin-fold window chambers; see main text for dosing schedule. A) shows images of the vasculature under transmitted light conditions using a x10 objective from 2 regions of interest (ROI) in a single representative tumor from each group (see Figure 4 for the tumor location of each region of interest); dotted lines demarcate tumor edges. Images on the far-right illustrate vessel demarcation for subsequent quantitation, using in-house-developed software, for the adjacent ROIs. B) shows quantitation of total vessel length per tumor area and average length of individual vessels derived from images such as shown in A); data are means ± 1 SEM for n = 5-7 tumors per group. C) shows quantitation of red blood cell velocity in individual blood vessels determined from video images captured under epi-fluorescence using a x20 objective from 2 ROIs

such as those shown in A); data are means ± 1 SEM for n = 5-7 tumors per group; data were acquired from approximately 20 vessels per ROI. * represents a significant difference between groups ($P < 0.05$; 1-way ANOVA followed by Tukey-Kramer post-hoc test).

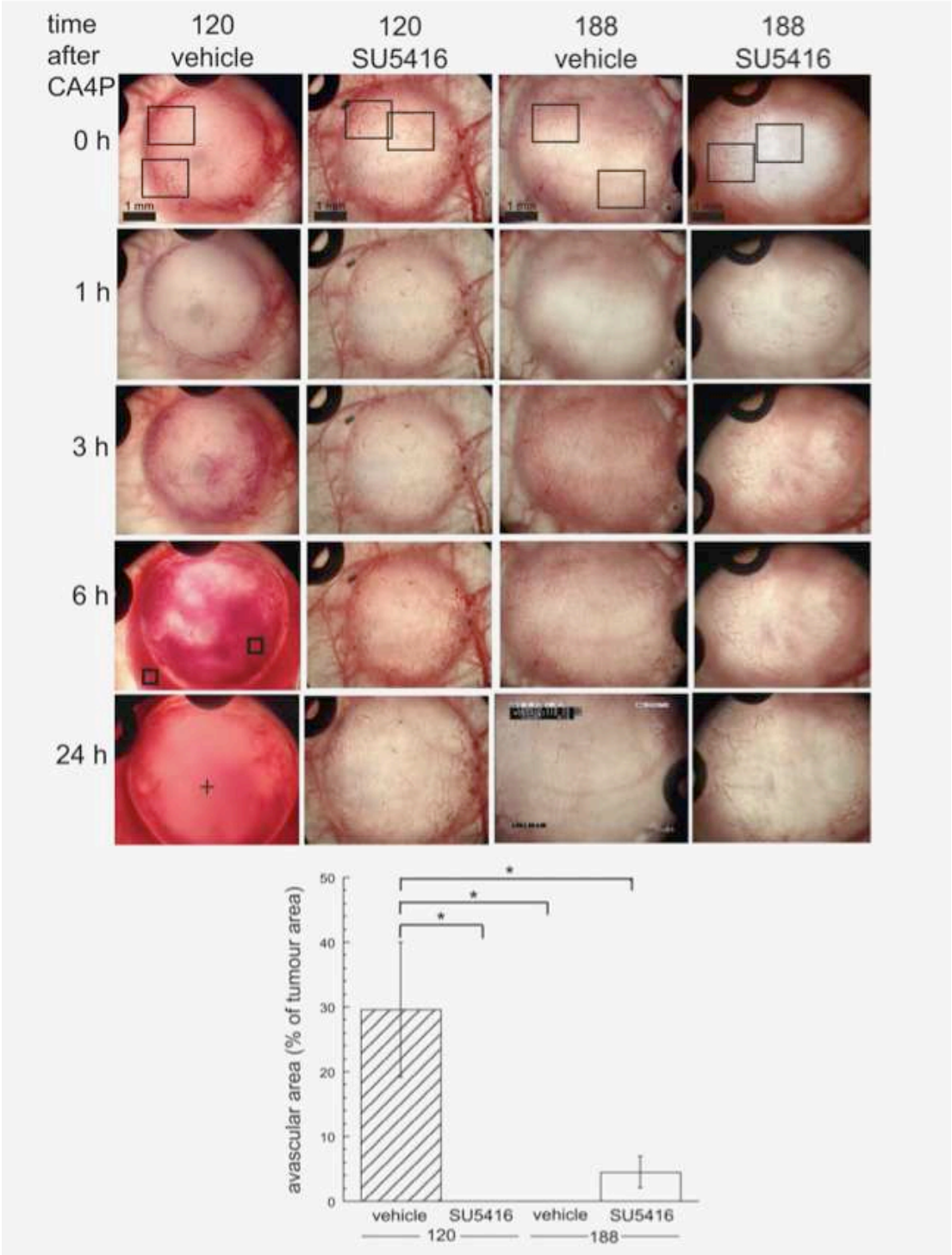

Figure 4

Representative low power images (x2.5 objective) of tumors growing in dorsal skin-fold window chambers before and after treatment with a single i.v. dose of CA4P (30 mg/kg), with/without chronic pre-treatment with SU5416 or vehicle. See main text for dosing schedules. Images at 0 h indicate the positions of the ROIs used for these tumors in the quantitative analysis of data shown in Figures 3 and 5. ◘ represents hemorrhage; + indicates a large avascular region occupying most of the tumor volume. Graph shows quantitation of the extent of central avascular regions at 24 h after CA4P treatment. There were no completely avascular regions in VEGF120 tumors treated with SU5416 or VEGF188 tumors treated with vehicle only. Data are means ± 1SEM; n = 5-7. * represents a significant difference between groups ($P < 0.05$; 1-way ANOVA followed by Tukey-Kramer post-hoc test).

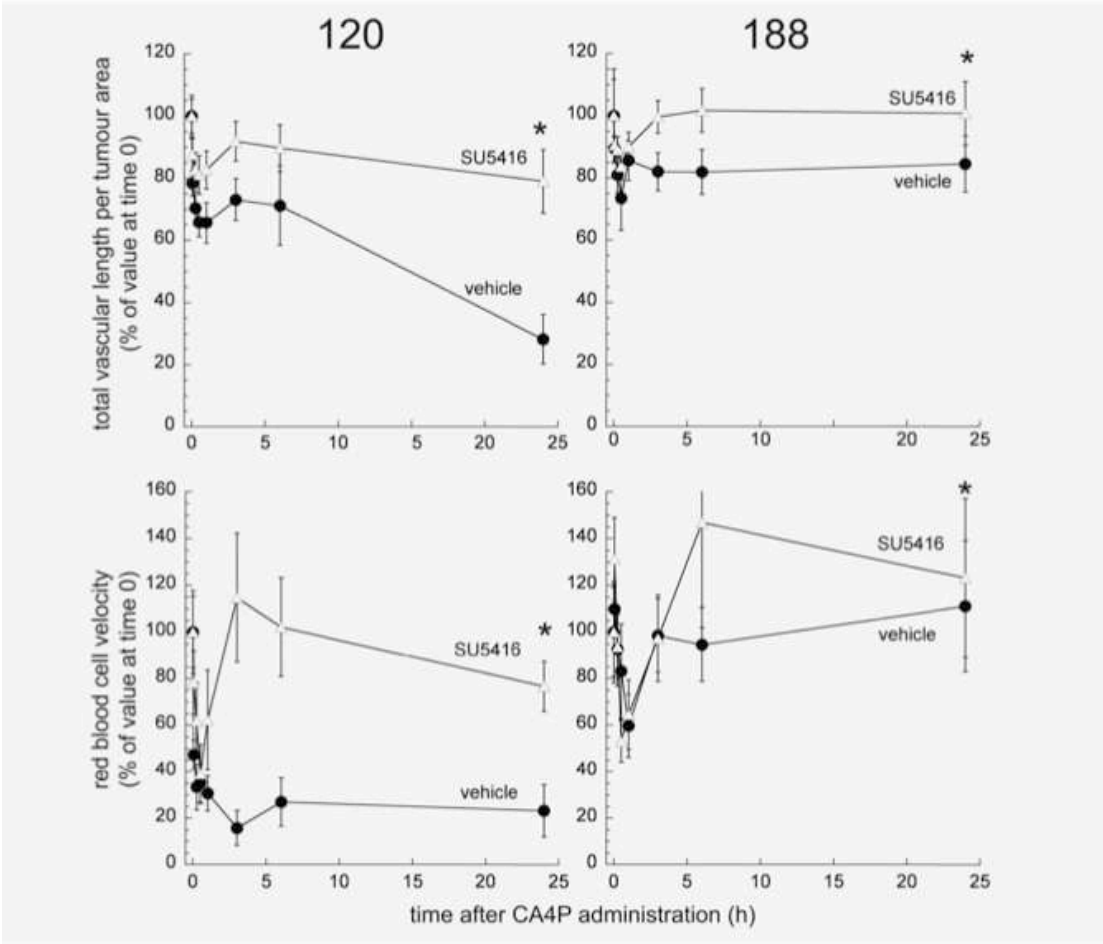

Figure 5

Effect of chronic pre-treatment with SU5416 on morphological and functional vascular response of VEGF120- and VEGF188-expressing tumors growing in dorsal skin-fold window chambers to a single i.p. dose of CA4P (30 mg/kg); see main text for dosing schedules. Both tumors were significantly more resistant to CA4P treatment if they had been pre-treated with SU5416. * represents a significant difference ($P < 0.05$) between the full time-course for SU5416 and vehicle pre-treatments (mixed design ANOVA with repeated measures). Data are means ± 1 SEM for n = 5-7 tumors per group.

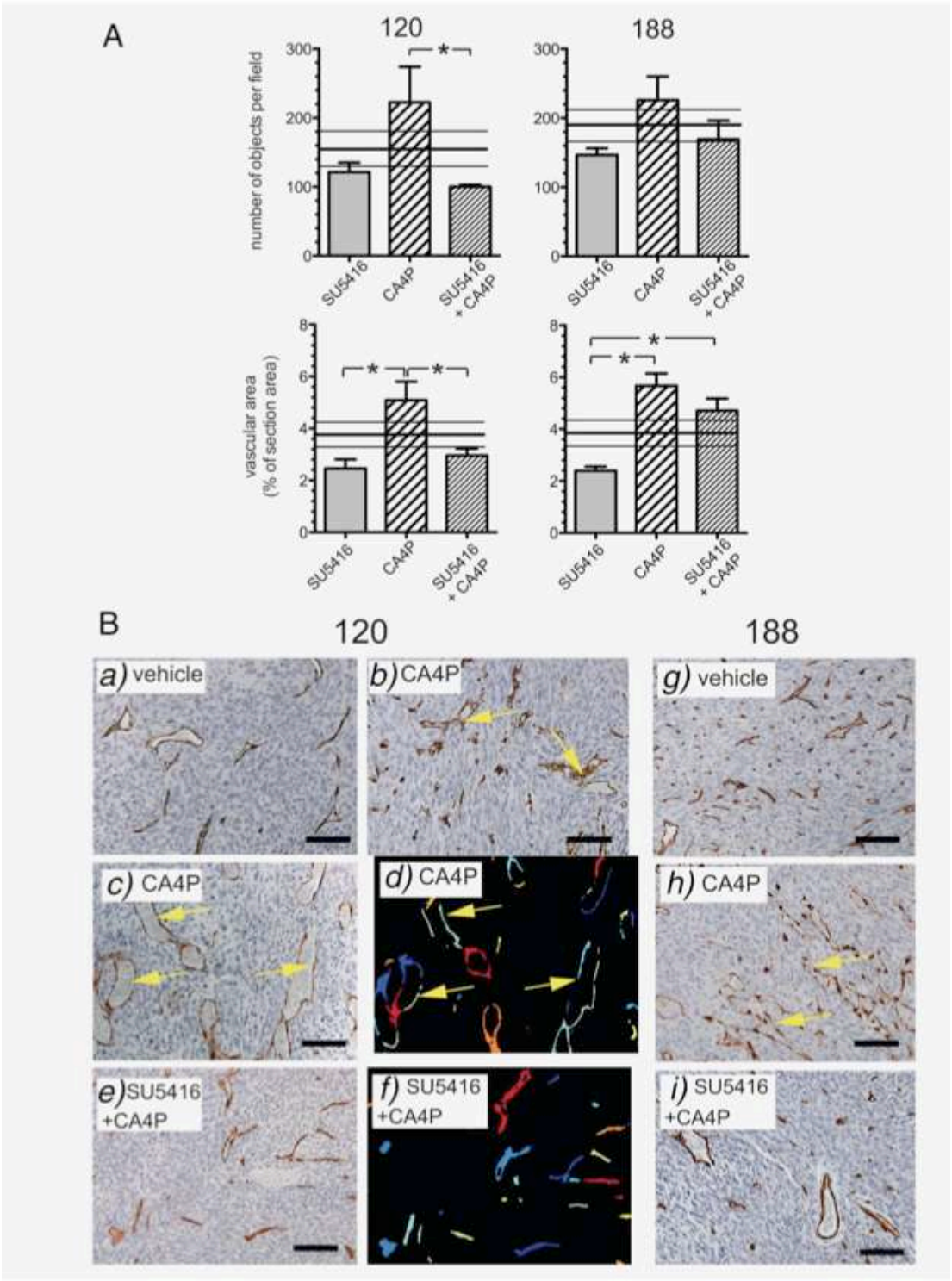

Figure 6

Effect of chronic pre-treatment with SU5416 on morphological vascular response of sub-cutaneous VEGF120- and VEGF188-expressing tumors to a single i.p. dose of CA4P (30 mg/kg); tumors were assayed 3 h after CA4P treatment, see main text for

dosing schedules. (A): Number of objects per field (as defined by CD31 staining) and vascular area (% pixels positive for CD31) in fixed tissue; * represents a significant difference between groups ($P < 0.05$, unpaired students' t-test). Data represent means ± 1 SEM for n= 4-7 per group; ≥ 7 ROIs per tumor; parallel lines represent mean ± 1 SEM for vehicle-treated tumors, as shown in Figure 1. (B) Example images from the different treatment groups showing CD31 staining in brown (x20 objective) and the corresponding computed vascular delineations for two of the images, where each colour represents a single object. Note that the software identified multiple objects from single vessels for the CA4P-treated tumor (yellow arrows), due to disrupted endothelial cell linings, whereas vessel identification is more accurate for the tumor pre-treated with SU5416. Scale bar represents 100 μm.